NEOPLASIA
www.neoplasia.com

Volume 13 Number 9 September 2011 pp. 831–840 **831**

Glioma Cell Migration on Three-dimensional Nanofiber Scaffolds Is Regulated by Substrate Topography and Abolished by Inhibition of STAT3 Signaling[1,2]

Paula A. Agudelo-Garcia[*,3], Jessica K. De Jesus[*,3], Shante P. Williams[†], Michal O. Nowicki[†], Ennio Antonio Chiocca[†], Sandya Liyanarachchi[‡], Pui-Kai Li[§], John J. Lannutti[¶], Jed K. Johnson[¶], Sean E. Lawler[†,4] and Mariano S. Viapiano[*,†]

*Center for Molecular Neurobiology, The Ohio State University, Columbus, OH, USA; [†]Dardinger Neuro-Oncology Center, Department of Neurological Surgery, The Ohio State University Medical Center and James Cancer Hospital, Columbus, OH, USA; [‡]Department of Biomedical Informatics, The Ohio State University Medical Center and James Cancer Hospital, Columbus, OH, USA; [§]Division of Medicinal Chemistry, The Ohio State University College of Pharmacy, Columbus, OH, USA; [¶]Department of Materials Science and Engineering, The Ohio State University College of Engineering, Columbus, OH, USA

Abstract

A hallmark of malignant gliomas is their ability to disperse through neural tissue, leading to long-term failure of all known therapies. Identifying new antimigratory targets could reduce glioma recurrence and improve therapeutic efficacy, but screens based on conventional migration assays are hampered by the limited ability of these assays to reproduce native cell motility. Here, we have analyzed the motility, gene expression, and sensitivity to migration inhibitors of glioma cells cultured on scaffolds formed by submicron-sized fibers (nanofibers) mimicking the neural topography. Glioma cells cultured on aligned nanofiber scaffolds reproduced the elongated morphology of cells migrating in white matter tissue and were highly sensitive to myosin II inhibition but only moderately affected by stress fiber disruption. In contrast, the same cells displayed a flat morphology and opposite sensitivity to myosin II and actin inhibition when cultured on conventional tissue culture polystyrene. Gene expression analysis indicated a correlation between migration on aligned nanofibers and increased STAT3 signaling, a known driver of glioma progression. Accordingly, cell migration out of glioblastoma-derived neurospheres and tumor explants was reduced by STAT3 inhibitors at subtoxic concentrations. Remarkably, these inhibitors were ineffective when tested at the same concentrations in a conventional two-dimensional migration assay. We conclude that migration of glioma cells is regulated by topographical cues that affect cell adhesion and gene expression. Cell migration analysis using nanofiber scaffolds could be used to reproduce native mechanisms of migration and to identify antimigratory strategies not disclosed by other *in vitro* models.

Neoplasia (2011) 13, 831–840

Abbreviations: TCPS, tissue culture polystyrene

Address all correspondence to: Mariano S. Viapiano, PhD, Department of Neurological Surgery and Center for Molecular Neurobiology, The Ohio State University Medical Center and James Cancer Hospital, 1060 Carmack Rd, Columbus, OH 43210. E-mail: viapiano.1@osu.edu

[1]This work was supported by grants from the National Institutes of Health (1R01CA152065-01 to M.S.V. and 1R43CA150763-01 to J.J.L. and J.K.J.) and the National Science Foundation (STTR 1010406 to J.K.J.). J.J.L. and J.K.J. hold Ohio State University–sponsored patent applications for the design of nanofiber-based scaffolds.
[2]This article refers to supplementary materials, which are designated by Tables W1 to W3 and Figures W1 to W6 and are available online at www.neoplasia.com.
[3]These authors contributed equally to this work.
[4]Dr Lawler is currently with the Leeds Institute of Molecular Medicine, St. James University Hospital, Leeds, United Kingdom.
Received 3 May 2011; Revised 15 July 2011; Accepted 21 July 2011

DOI 10.1593/neo.11612

Introduction

Cell migration away from the site of the primary tumor is a hallmark of malignant cancers often leading to recurrence and the failure of existing therapies. This is particularly evident in malignant gliomas, the most challenging tumor of the central nervous system characterized by its ability to disperse through normal neural tissue and recur after initial treatment [1].

Histologic evidence has shown that glioma cell dispersion in the brain occurs along preferential patterns, in many cases following the orientation of thin, elongated anatomic structures such as capillaries, white matter fibers, and unmyelinated axons [2]. Unfortunately, standard assays devised to study glioma cell motility do not incorporate such topographical cues guiding cell adhesion and traction *in vivo*, focusing instead on cell motility on either rigid (i.e., polystyrene or glass) surfaces or invasion through a homogeneous, collagen-based matrix that is absent in neural tissue [3,4].

Motile glioma cells are more resistant than nonmotile cells to apoptotic stimuli [5,6], and current evidence suggests that conventional therapies may in fact trigger glioma cell dispersion [7,8]. Thus, understanding the mechanisms of glioma cell migration is critical to the development of more efficient targeting strategies as part of adjuvant therapy. Antimigratory approaches against gliomas have targeted cell adhesion molecules or tumor-associated proteases, following antimetastatic strategies used in other solid tumors [9]. However, these approaches have been largely ineffective in the clinical setting, partly because of the ability of brain tumor cells to shift between different mechanisms of cell adhesion as well as proteolytic and nonproteolytic modes of migration [3,10]. This underscores the need for additional studies to identify antimigratory compounds capable of targeting the master regulators of tumor cell locomotion [3].

In a recent study, we demonstrated that glioma cells can be cultured on scaffolds made of poly-ε-caprolactone nanofibers produced by electrospinning [11]. Fiber density, alignment, and stiffness can be controlled in these scaffolds, thus providing the cells with a topographically complex substrate. Glioma cells were able to grow on nanofibers of different alignment and accurately reproduced the morphologies described for these cells migrating through neural tissue [10,12]. Here, we show that migration of glioma cells on nanofiber scaffolds reproduces not only the morphology but also characteristic molecular features of three-dimensional migration and results in a pattern of gene expression dependent on fiber alignment. Moreover, we show that active cell migration on aligned nanofibers correlates with activation of the transcription factor STAT3, a central regulator of tumor progression and metastasis in solid cancers [13]. Accordingly, subtoxic inhibition of STAT3 specifically reduced glioma cell migration on nanofibers, suggesting that this novel culture technology could be used for screening of antimigratory compounds.

Materials and Methods

Preparation of Nanofiber-Coated Culture Plates

Poly-ε-caprolactone nanofibers were prepared as previously described [11] with minimal modifications. Briefly, optically clear polystyrene film (thickness, 190 μm; MultiPlastics, Inc, Lewis Center, OH) was cut to the desired final size and attached to the side of a rotating drum (Nanofiber Solutions, Columbus, OH). Nanofibers were deposited by electrospinning, using a syringe perpendicular to the polystyrene film as described [11]. Fiber alignment was controlled by the rotational speed of the drum and scaffold thickness by the amount of time used to deposit the nanofibers. Films covered with multilayered nanofiber scaffolds were trimmed, attached to bottomless culture plates (Figure 1*A*), and sterilized with UV radiation (350 mJ/cm^2) before use.

Cell Cultures and Reagents

The human glioma cell lines U87 and U251 (American Type Culture Collection, Manassas, VA) were grown at 5% CO_2 in Dulbecco modified Eagle medium supplemented with 10% fetal calf serum. The identity of these cells was confirmed through "Cell Check" authentication service provided by the Research Animal Diagnostic Laboratory (Columbia, MO). Two cultures of glioblastoma-derived tumor initiating cells (G8 and G9) were prepared from freshly resected tumors and cultured as neurospheres in serum-free medium as described [14]. These cells have been characterized as tumor stem cells elsewhere [15], display self-renewal *in vitro*, and are highly tumorigenic *in vivo*, replicating the phenotype of the original tumors. Only low passages of G8 and G9 cells (up to five passages) were used.

To prepare tumor xenografts, G8 and G9 cells were implanted in the striatum of athymic mice as described [16]. After 2 weeks, animals were perfused with saline, and tumors were resected and minced in Hank's balanced salt solution. Tissue explants were cultured in suspension in neurosphere medium for 72 hours, with daily changes of medium to remove debris. Explants containing viable tumor cells were detected by uptake of the fluorescent dye calcein-AM (5 μM; Invitrogen, Carlsbad, CA) and deposited on nanofiber scaffolds. As an alternative strategy, cells were first stably transduced with the lentiviral vector pCDH-EF1-coGFP (System Biosciences, Mountain View, CA) and used to generate tumors as above. Tissue pieces containing GFP-expressing tumor were processed under a fluorescence dissection microscope, cleaned of debris in Hank's balanced salt solution, and deposited on nanofiber scaffolds. Patterns of cell migration out of tissue explants were undistinguishable using either approach.

To inhibit cell migration, glioma cells were treated with the myosin II inhibitor blebbistatin (Sigma-Aldrich, St Louis, MO) and the actin polymerization inhibitor cytochalasin D (Sigma-Aldrich). To test the involvement of STAT3 on migration, cells were treated with the STAT3 inhibitors stattic (Tocris Bioscience, Ellisville, MO) [17] and LLL12 (Division of Medicinal Chemistry, Ohio State University, Columbus, OH) [18]. Cell viability was determined using an assay for reduction of soluble tetrazolium (CellTiter kit; Promega, Madison, WI).

Adhesion and Migration Assays

To quantify cell adhesion to nanofibers, glioma cells were dissociated and plated (30,000 cells/200 μl) in triplicate on nanofiber-coated or tissue culture polystyrene (TCPS) plates. After 30 minutes at 37°C, cells were washed, fixed, and quantified as described [19].

To analyze cell migration on nanofibers, 50,000 to 75,000 glioma cells were plated on 35-mm agar plates to form spheroids [16]. After 48 hours, glioma spheroids 200 to 250 μm in diameter were stained with 5 μM CellTracker CMFDA (Invitrogen) and manually placed within nanofiber-coated wells. To analyze the migration of glioblastoma-derived initiating cells, either from neurospheres or from tumor explants, nanofibers were first precoated with 5 μg/ml fibronectin in phosphate-buffered saline for 2 hours. Migration index was calculated as the ratio of maximum dispersion (Figure W1*A*) divided by the original diameter of the spheroids.

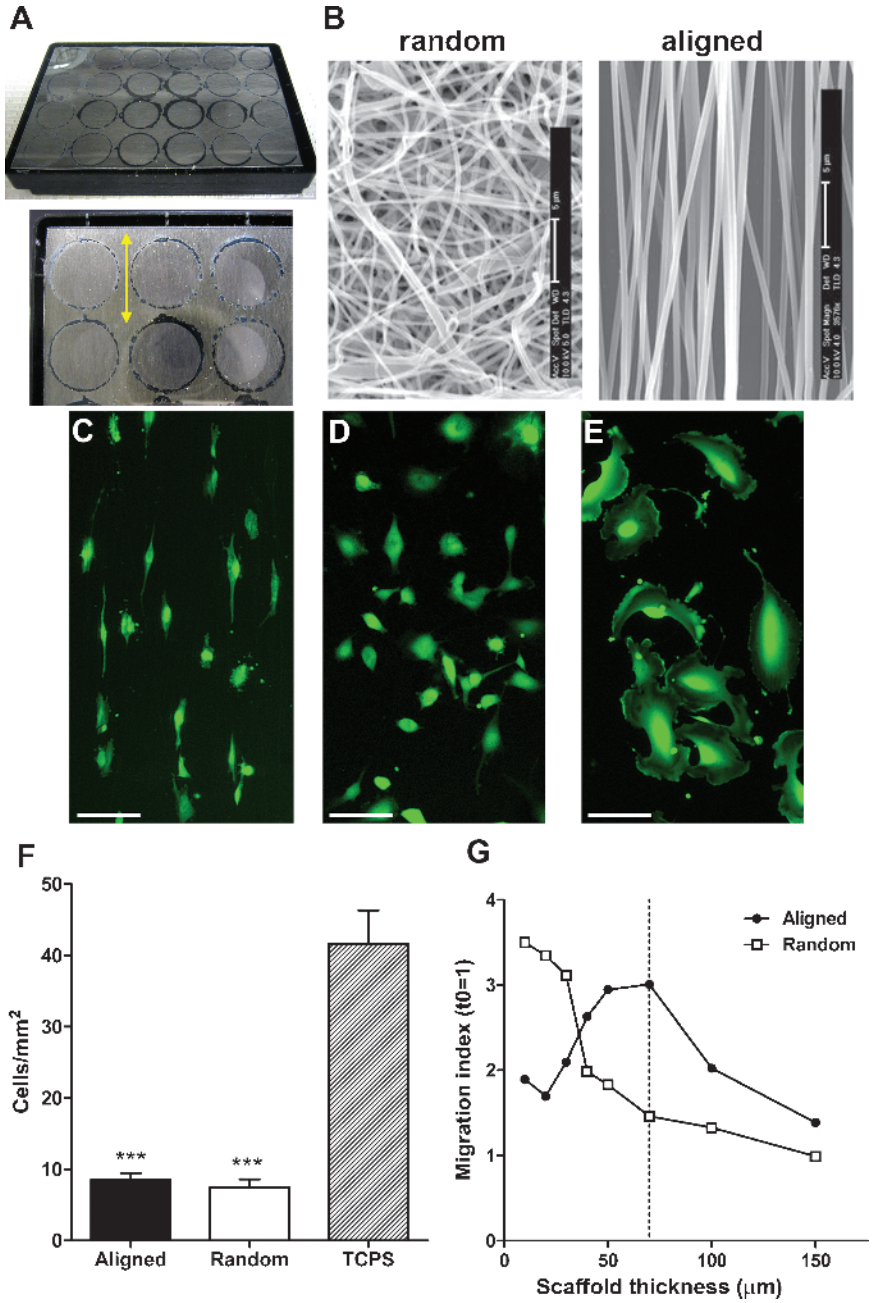

Figure 1. Glioma cell morphology and migration are directed by substrate topography. (A) Representative photography of a multiwell culture plate with a nanofiber-coated backing film. The enlarged image shows the translucent coating of nanofibers, and the double-headed arrow indicates the direction of fiber alignment. (B) Scanning electron microscope images of randomly oriented and highly aligned nanofibers. Bars, 5 μm. (C-E) Images of calcein-stained U251 glioma cells cultured on highly aligned nanofibers (C), randomly oriented nanofibers (D), or conventional TCPS (E). Bars, 100 μm. (F) Quantification of cell adhesion (U251 cells/mm^2) showed significantly lower adhesion of cells to nanofibers compared with TCPS (***$P < .001$), but no differences between randomly oriented and aligned nanofibers (analysis by one-way ANOVA and Bonferroni *post hoc* tests). (G) Radial dispersion of U251 cells from cell aggregates was measured using nanofiber scaffolds of different thickness. Cells gained motility much faster on aligned than on randomly oriented nanofibers as the fibers became sparser. Use of 70-μm-thick scaffolds (dashed line) resulted in the highest cell motility on aligned nanofibers but little motility of the same cells on randomly oriented nanofibers.

To analyze cell migration on TCPS plates, glioma cells were tested using conventional wound healing and radial dispersion assays as previously described [20]. To analyze cell translocation ("Transwell assay"), 30,000 cells were applied to uncoated cell culture inserts with 8-μm pores (Greiner Bio-One, Monroe, NC). Migration in response to a chemoattractant gradient (0%-10% serum) was measured after 8 hours by counting the number of transmigrated cells.

To analyze cell migration using an organotypic culture model, cultures of mouse neonatal brain slices were prepared as we have previously described [16]. Aggregates of GFP-expressing glioma cells were pretreated overnight with STAT3 inhibitors, deposited on the tissue slices, and followed by fluorescence microscopy for up to 96 hours. Dispersion was quantified by analyzing the total area and perimeter covered by the migratory cells [16].

All experiments of cell migration were performed three times with at least three independent replicates per condition except brain slice experiments, which used eight replicates.

Microarray Experiments

To compare gene expression of glioma cells migrating on aligned *versus* randomly oriented nanofibers 5×10^5 U251 cells were cultured in nanofiber-coated 60-mm culture plates, collected after 48 hours, and processed with TRIzol (Invitrogen) according to standard protocols. Total RNA from independent triplicates was processed for hybridization to Affymetrix U133+ 2.0 microarrays at The Ohio State University Microarray Shared Resource. Data were deposited in the National Center for Biotechnology Information's Gene Expression Omnibus Repository for Functional Genomic Studies (data set GSE28167). Significantly upregulated genes (>1.5-fold; Table W1) in cells cultured on aligned nanofibers were analyzed using Ingenuity Pathway Analysis to identify top functional networks and DAVID bioinformatics resources to identify top functional clusters (Table W2). Quantitative reverse transcription–polymerase chain reaction (RT-PCR) was performed in parallel samples to verify the expression level of selected messenger RNA (primers listed in Table W3).

Western Blot Analysis

Dissociated U251 and G9 cells cultured in nanofiber-coated 60-mm culture plates were lysed *in situ* in 20 mM Tris-HCl buffer, pH 7.6, containing 150 mM NaCl, 1% vol/vol NP-40, 0.5% vol/vol sodium deoxycholate, and protease plus phosphatase inhibitors (Complete and PhosSTOP cocktails; Roche Applied Science, Indianapolis, IN). Proteins were processed for Western blot analysis with antibodies against STAT3 and phospho-Tyr^{705} STAT3 (Cell Signaling Technology, Danvers, MA), myosin light chain 2 (MLC2) and phospho-Ser^{19} MLC2 (Cell Signaling), and β-tubulin (Sigma-Aldrich).

Statistical Analysis

Cell adhesion and translocation experiments were analyzed by one-way analysis of variance (ANOVA) followed by *post hoc* Bonferroni tests. Cell migration on nanofibers, TCPS, or brain slices was analyzed by two-way ANOVA for repeated measures. Results of STAT3 inhibition on nanofibers were analyzed by one-way ANOVA for each inhibitor and cell type. $P < .05$ indicates significant differences between treatments. Bar graphs in the figures represent mean ± SD. Microarray data were analyzed by robust multichip average procedure using quantile normalization. Differentially expressed genes between two groups were identified with a modified *t* test [21] using BRB-Array Tools software.

Results

Glioma Cell Morphology and Migration Depend on Fiber Alignment

To better understand the mechanisms underlying glioma cell migration in response to variable topographical cues, we first analyzed the morphology and behavior of glioma cells cultured on three-dimensional nanofiber scaffolds *versus* conventional two-dimensional surfaces. Dissociated U251 glioblastoma cells were plated on conventional TCPS plates and compared against cells cultured on two distinct types of nanofiber scaffolds (50 μm thick; Figure 1, *A* and *B*). Cells cultured on aligned nanofibers adopted a fusiform morphology, usually with a leading process following an individual fiber (Figure 1*C*). In contrast, cells on randomly oriented fibers remained relatively rounded (Figure 1*D*). In neither case did we see obvious lamellipodia or fan-shaped morphologies that were typical of these cells cultured on TCPS (Figure 1*E*). Despite their different morphologies, initial cell adhesion was similar on both types of nanofiber substrates, although considerably lower than adhesion to TCPS (Figure 1*F*).

Next, we quantified cell migration on nanofibers using a radial migration assay to measure cell dispersion out of a tumor aggregate or "core" [11,20] (Figure W1*A*). Glioma cell spheroids were plated on nanofiber scaffolds of different thickness (10-200 μm) to determine the effect of fiber density on cell migration. We observed that cell migration was very restricted at the highest fiber densities and, as expected, increased as the nanofibers became sparser (Figures 1*G* and W1*B*). Interestingly, migration on highly aligned nanofibers peaked on relatively thick scaffolds (60-80 μm), whereas migration on randomly oriented nanofibers remained low until the fibers were very sparse (<30 μm thick), which likely allowed the cells to contact the underlying substrate [11]. Therefore, we chose 70-μm-thick nanofiber scaffolds for our subsequent experiments to provide maximum differences in total cell motility between the two different types of fiber orientations.

Glioma Cell Migration on Aligned Nanofibers Is Myosin II Dependent

Recent work has shown that cell motility in a three-dimensional environment is a substantially different process from migration on rigid two-dimensional surfaces, being less dependent on focal adhesions and long, anchored, stress fibers and more on the local contraction of actomyosin complexes to squeeze the tail-end of the cell through intercellular spaces [10,22]. To determine whether migration of glioma cells on nanofiber scaffolds reproduced this key molecular feature of three-dimensional migration, we assessed the effect of inhibitors targeting myosin II and actin polymerization on cell migration.

Migration of U251 glioma cells out of aggregates seeded on aligned nanofibers was significantly inhibited by the myosin II inhibitor blebbistatin (Figure 2, *A* and *B*). However, blebbistatin did not affect glioma cells on randomly oriented nanofibers, where motility was already restricted. When we compared these results with a conventional cell translocation assay where the cell body must be squeezed through the pores of culture inserts, we observed that blebbistatin partially inhibited the translocation of glioma cells but at a considerably higher concentration than that needed to inhibit cell migration on nanofibers (Figure 2*C*). In contrast, in a conventional wound healing assay (Figure 2*D*), glioma cell migration was not affected by blebbistatin, in agreement with the literature [10]. Overall, these results suggested that cell motility on aligned nanofibers was highly dependent on myosin II activity as in other three-dimensional models.

On the other hand, the inhibitor of actin polymerization cytochalasin D was much less effective in inhibiting cell motility on nanofibers compared with the same cells plated on TCPS. Cytochalasin D treatment of U251 cells caused some disruption of cortical F-actin, visualized as appearance of punctuate actin staining (Figures 3*A* and W2). However, cell dispersion on aligned nanofibers was only reduced significantly ($P < .01$) when U251 cells were exposed to toxic concentrations of this inhibitor (>2 μM). In comparison, dispersion of the same glioma cells on TCPS, measured with a radial migration assay (Figure 3*B*) or a wound healing assay (Figure W2), was significantly reduced ($P < .001$) at the lowest concentration of cytochalasin D tested (0.2 μM), and cells not only stopped migrating but also detached from the plates at a 2-μM concentration of this inhibitor. These results

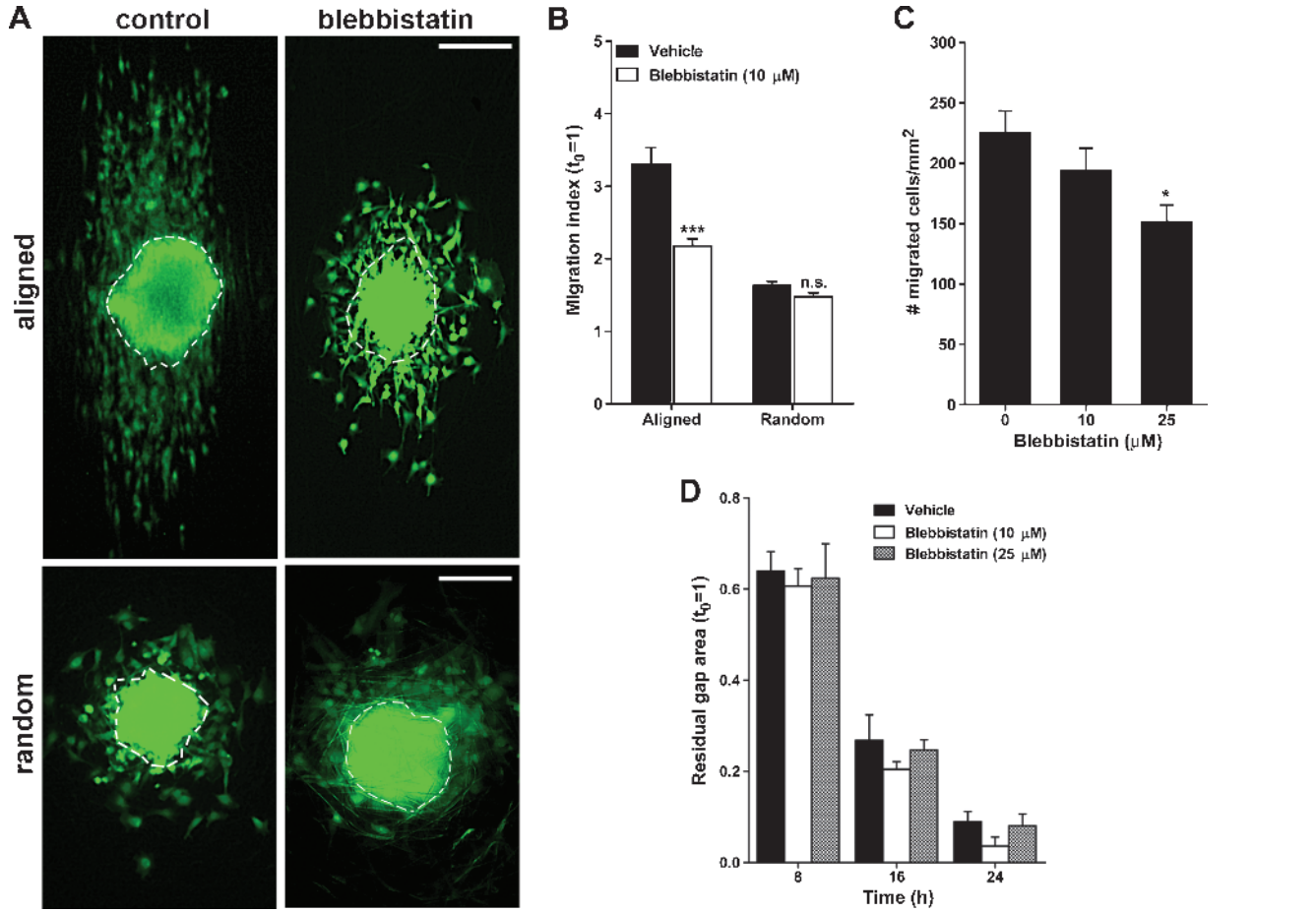

Figure 2. Glioma cell migration on aligned nanofibers is myosin II–dependent. (A) Representative images of U251 glioma cell aggregates after being cultured for 24 hours on aligned or randomly oriented nanofibers, in the presence of 10 μM blebbistatin (blebbistatin) or its vehicle (control). Notice the parallel and elongated migration profile of cells on aligned nanofibers. Dashed outlines indicate the size and shape of the same aggregates at $t = 0$ h. Bars, 200 μm. (B) Effect of blebbistatin on cell dispersion on nanofibers. Results indicate a significant inhibition of cell migration on aligned but not on randomly oriented nanofibers. ***$P < .001$ by two-way ANOVA. (C) Effect of blebbistatin on cell translocation through cell culture inserts. Results indicate a significant effect only at 25 μM blebbistatin. *$P < .05$ by one-way ANOVA and Bonferroni *post hoc* test. (D) Effect of blebbistatin on two-dimensional cell migration measured with a wound healing assay. Migration of U251 cells in this assay was not affected by the myosin II inhibitor.

suggested that, while actin polymerization was still required for cell migration on nanofibers, the formation of long stress fibers was less critical than for motility of a rigid surface [23]. Together, the results from acto–myosin II disruption suggested that cell migration on nanofibers reproduced more closely the molecular features observed on three-dimensional migration rather than those observed for migration on rigid two-dimensional surfaces.

Cell Migration on Aligned Nanofibers Results in Elevated JAK/STAT Signature

Both here and in a previous study [11], we have observed a substantial difference in the behavior of glioma cells cultured on aligned nanofibers, where the cells migrate efficiently, *versus* randomly oriented nanofibers, where migration is highly restricted without evident effects on viability. Therefore, we investigated whether the different migratory behavior of glioma cells that were otherwise equivalent for viability [11] or adhesion (Figure 1*F*) was reflected in differential gene expression.

Using microarray analysis to compare U251 glioma cells cultured on aligned *versus* randomly oriented nanofibers, we observed significant differences in gene expression (summarized in Table W1). Pathway and gene ontology analysis suggested a strong association between the genes upregulated in cells cultured on aligned nanofibers and functional clusters involved in positive regulation of cell motility (Table W2). Strikingly, there was a remarkable up-regulation of genes that are known activators or targets of JAK/STAT signaling [24–26], including *IL8*, *IL11*, *TLP*, *CXCL2*, *CCND1*, *PIK3CD*, *SPHK1*, *PIK3CD*, and *SERPINE1*. Up-regulation of these genes in cells cultured on aligned nanofibers was subsequently validated by quantitative RT-PCR (Figure 4*A*).

Because these results suggested a possible involvement of STAT signaling in glioma cell migration, we focused on the transcription factor STAT3, which has been recently highlighted as a central regulator of malignant progression in high-grade gliomas [27]. In agreement with our results of gene expression, Western blot analysis results showed that the active phosphorylated form of STAT3 was markedly increased in cells cultured on aligned nanofibers shortly after the cells attached to the substrate, whereas it was barely detectable in cells on randomly oriented nanofibers, even after

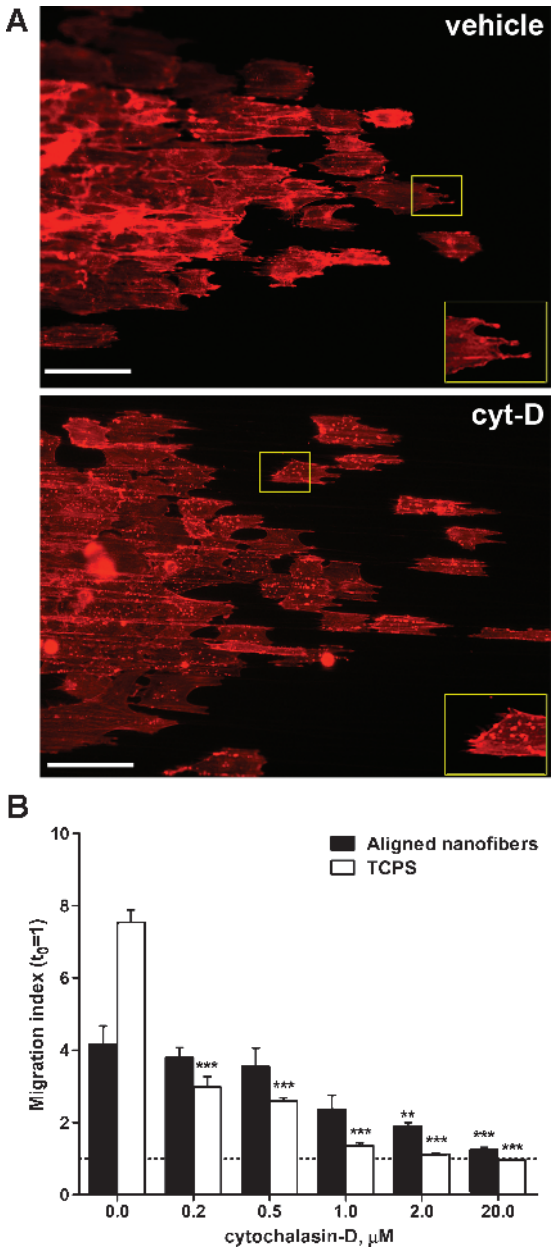

Figure 3. Cell migration on nanofibers is less sensitive to stress fiber disruption than two-dimensional migration. (A) U251 glioma cell aggregates were cultured on aligned nanofibers, fixed after 24 hours, and stained with phalloidin–Alexa 594 to label actin F. Results show diffuse cortical staining in vehicle-treated cells (vehicle) *versus* punctuate staining (insets) along actin filaments in cells treated with the actin polymerization inhibitor cytochalasin D (cyt-D, 2 μM). Cell morphology was little or not affected in these conditions. Bars, 100 μm. (B) Quantification of radial dispersion of U251 cells shows that two-dimensional cell dispersion on TCPS was significantly reduced even at the lowest concentration of cytochalasin D tested (0.2 μM), whereas dispersion on nanofibers required 10 to 100× higher concentrations to be significantly inhibited. $^{**}P < .01$, $^{***}P < .001$ by one-way ANOVA for each treatment.

24 hours in culture (Figure 4*B*). In agreement with previous literature [28–30], active phosphorylated STAT3 was also highly expressed in glioma cells cultured on TCPS, where cell motility is unimpeded by the substrate.

Inhibition of STAT3 Reduces the Migration of Glioma Cells on Nanofiber Scaffolds

To determine whether cell migration on nanofibers could be used as a model to analyze the role of STAT3 on glioma cell migration, we tested two STAT3 inhibitors that specifically prevent STAT3 phosphorylation of Tyr^{705}, a critical residue necessary for STAT3 dimerization and transcriptional activity. Both inhibitors, stattic and LLL12, significantly inhibited the migration of U251 cells cultured on aligned nanofibers (Figures 5, *A* and *B*, and W3), at concentrations (0.5-2.0 μM) that did not affect cell viability during these short assays (Figure W4). These results were reproduced with an additional glioma cell line (U87) and two preparations of primary glioblastoma-derived initiating cells (G8 and G9); all of them tested on aligned nanofibers. Moreover, the inhibition of cell migration matched the reduction or complete inhibition of STAT3 phosphorylation by these compounds (Figure 5, *C* and *D*).

Interestingly, these subtoxic concentrations of stattic or LLL12 were unable to inhibit cell motility when tested in a conventional wound healing assay (Figure 5*E*), suggesting that the inhibitors had disrupted a sensitive mechanism necessary for cell migration in three-dimensional nanofiber scaffolds but not on rigid two-dimensional surfaces. In agreement, the phosphorylation of STAT3 and MLC2, a regulatory chain of myosin II necessary for myosin activity, were significantly reduced in cells treated with a low concentration of stattic on aligned nanofibers but not on polystyrene dishes (Figure W5). Together with our results showing that myosin II activity was critical for cell migration on aligned nanofibers (Figure 2), these results suggested that actomyosin activity on nanofibers, but not on TCPS, was finely regulated by STAT3 and highly sensitive to partial STAT3 inhibition. The sensitivity of glioma cell migration to low concentrations of STAT3 inhibitors was also observed in cells dispersing in cultured brain slices, a complex three-dimensional environment reproducing the natural cytoarchitecture and natural barriers to cell movement in the brain (Figure W6), suggesting that cell migration on nanofibers was supported by similar or the same mechanisms as in complex three-dimensional organotypic cultures. In contrast, inhibition of STAT3 did not reduce cell translocation in a Transwell migration assay at low concentrations of inhibitors (not shown) and had only a partial effect at high concentrations (LLL12 > 10 μM) that likely affected cell viability to some extent [18].

Because culture of tumor-derived neurospheres on nanofiber scaffolds required minimal processing steps and was highly reproducible, we finally asked if this culture model could be used to analyze cell migration directly out of fresh, biopsy-like tissue explants. We generated intracranial tumor xenografts using primary glioblastoma cells and recovered the tumors as well as adjacent brain tissue after 2 weeks. Viable tumor pieces, identified by calcein uptake or GFP fluorescence as indicated in the methods section, were minced, cleared of debris, and plated on fibronectin-coated aligned nanofibers. Cell migration took longer to be detected than migration out of homogeneous tumor neurospheres, but there was consistent glioma cell migration out of the tissue explants and along aligned nanofibers within 48 to 72 hours (Figure 6*A*). More importantly, treatment of the tumor explants with the two STAT3 inhibitors reduced significantly or abolished the outward migration of glioma cells (Figure 6*B*).

Taken together, our results revealed a possible role for STAT3 in the migration of glioma cells in response to topographical cues and demonstrated the advantages of three-dimensional nanofiber scaffolds as a culture model to investigate pathways involved in cancer cell migration.

Discussion

Malignant gliomas have a very poor prognosis owing to their extensive infiltration of the surrounding normal neural tissue [2]. This infiltration is triggered in part by chemotherapy and radiotherapy [7,8,31], and motile glioma cells are highly resistant to these treatments [5,32]. Thus, understanding the mechanisms that drive glioma cell motility may improve not only the development of anti-invasive strategies but also the efficacy of current adjuvant therapies.

In this context, a major problem in studying cell motility *in vitro* is the difficulty of reproducing the native behavior of these tumor cells. With few exceptions [9], assays to study glioma cell invasion have largely reproduced the models used to study motility of other epithelial solid tumors, such as the wound healing assay (two-dimensional motility) and invasion through collagen-based matrices (three-dimensional motility) [9]. Glioma cells in these assays are exposed to a uniform environment—either an infinite flat surface or a uniform matrix—that lacks directional mechanical cues relevant to native mechanisms of cell migration in the brain. In response to limitations of other models, we developed a topographically complex environment for cell culture, using biocompatible scaffolds formed by electrospun submicron-sized fibers [11]. These scaffolds have mechanical properties, such as a low-tensile modulus (~7 MPa), comparable with those of biologic tissues [33] and are therefore highly compliant compared with tissue culture polystyrene (tensile modulus ~3600 MPa). This has allowed us to challenge glioma cells with a deformable substrate containing variable topography and analyze the molecular mechanisms involved in cell migration under these conditions.

Glioma cells adhered to nanofibers with less efficiency than to conventional TCPS, possibly due to less resistance from the substrate for the formation of focal adhesions [34,35], but total adhesion was independent of substrate topography (Figure 1*F*). In contrast, the actual migration of the cells was tightly dependent on the properties of the substrate, including both nanofiber alignment and density. Although the cells were not embedded in a matrix, we have previously shown that they can crawl through or become entangled in several layers of fibers [11]. The substrate is therefore irregular enough for the cells to exhibit three-dimensional migratory patterns, such as the marked body alignment and formation of protrusions along fibers, mimicking the formation of protrusions through the pores of a matrix and the elongated appearance of glioma cells migrating *in vivo* [10,36]. Furthermore, our data suggest that cell motility in nanofibers reproduced, at least in part, molecular features of three-dimensional

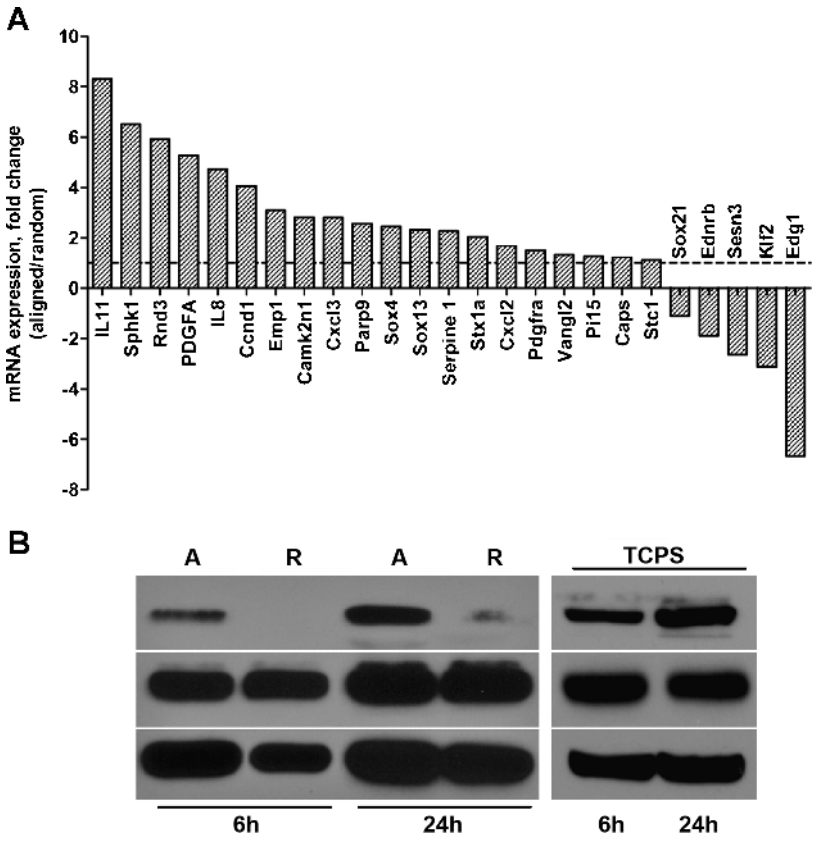

Figure 4. Glioma cell migration on aligned nanofibers correlates with activation of STAT3 signaling. (A) Quantitative RT-PCR results showing differential gene expression levels in glioma cells cultured on aligned *versus* randomly oriented nanofibers (selected genes are a subset of those listed in Table W1). Many of the upregulated genes are known modulators or targets of JAK/STAT and are involved in positive regulation of cell migration (Table W2). (B) Dissociated U251 glioma cells (5×10^5 cells/ml) were plated on aligned (A) or randomly oriented (R) nanofibers and collected 6 or 24 hours after attachment. Cells recovered from aligned nanofibers showed a substantial increase in Y^{705}-phosphorylated STAT3 (p-STAT3) compared with cells recovered from randomly oriented nanofibers. As a control, U251 cells were plated on conventional TCPS and processed in the same manner, showing considerable expression of total and active STAT3 at all times tested.

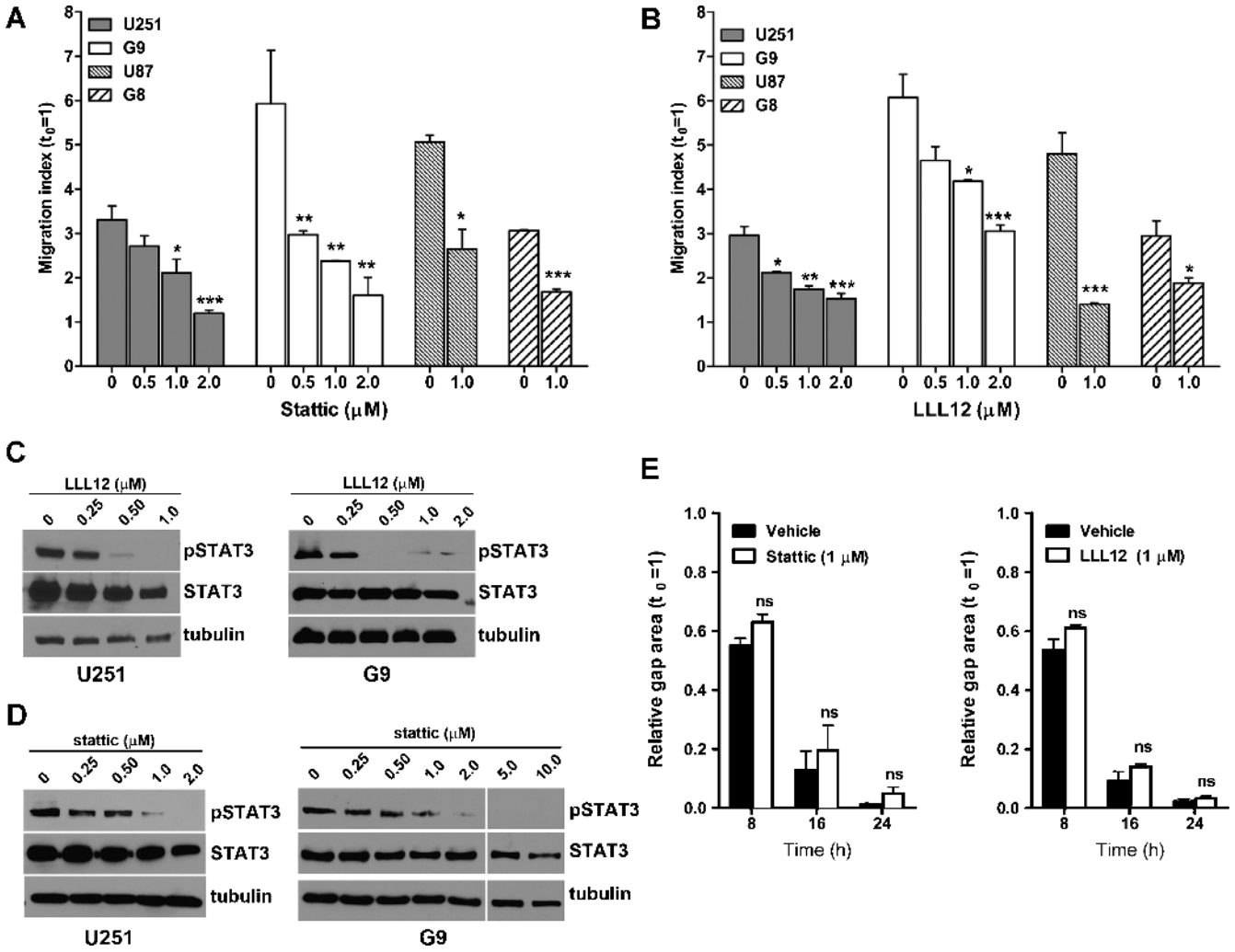

Figure 5. STAT3 inhibition reduces glioma cell migration on aligned nanofibers. (A and B) Cell dispersion was measured for two glioma cell lines (U251 and U87) and neurospheres from two glioblastoma-derived initiating cells (G8 and G9), in the presence of the STAT3 inhibitors stattic (A) and LLL12 (B). Both inhibitors significantly reduced cell migration at concentrations between 0.5 and 2 μM. *$P < .05$, **$P < .01$, ***$P < .001$ by one-way ANOVA for each cell type and inhibitor. (C and D) Western blot analysis of U251 and G9 cells collected from aligned nanofibers confirmed the inhibition of STAT3 phosphorylation (pSTAT3) using LLL12 (C) and stattic (D) at the same concentrations used to inhibit cell dispersion. STAT3 inhibition in G9 cells—which form large compact tumorspheres—was sometimes incomplete at low concentrations of LLL12 or stattic, but cell motility was, nevertheless, reduced. Complete STAT3 inhibition was achieved at higher concentrations of these inhibitors. (E) Migration of U251 cells using a wound healing assay was not affected by low concentrations of STAT3 inhibitors. NS indicates nonsignificant.

motility such as stringent myosin II dependence [10] and low sensitivity to disruption of stress fibers [23], which contrasted with the opposite features of the cells cultured on rigid two-dimensional surfaces.

Using an optimal combination of nanofiber density and alignment to promote (aligned nanofibers) or restrict (random nanofibers) cell dispersion, we demonstrated a substantial up-regulation of STAT3 signaling in migratory glioma cells on nanofibers. The transcription factor STAT3 is a key regulator of development and metastasis in solid tumors [13,37] and has been recently proposed as a major driver of glioblastoma progression [27]. STAT3 promotes glioma stem cell proliferation and pluripotency [38] and drives tumor development toward an aggressive mesenchymal phenotype [27], therefore being a target with significant clinical potential [39]. Indeed, down-regulation of STAT3 efficiently reduces glioma cell proliferation, induces apoptosis, and inhibits tumor growth *in vivo* [40–42]. This has prompted the recent development of novel small-molecule therapeutic agents targeting STAT3 in brain tumors [43,44].

Because the down-regulation of STAT3 in gliomas causes rapid cell death *in vitro*, the role of this transcription factor in glioma cell migration has not been extensively explored. de la Iglesia et al. [45] have reported that overexpression of constitutively activated STAT3 reduced glioma cell migration, possibly due to repression of interleukin 8 (IL-8) signaling. However, because STAT3 is known to activate IL-8 expression in other cell models [46,47] and is in turn regulated by IL-8 and other cytokines [48], this paradoxical effect of STAT3 could have been caused by an overexpressed construct lacking regulatory feedback in transfected cells. In contrast, recent studies have suggested that inhibition of STAT3 reduces glioma cell migration [18,30,49], although that effect was achieved in most cases using conditions that induced cell apoptosis at the same time.

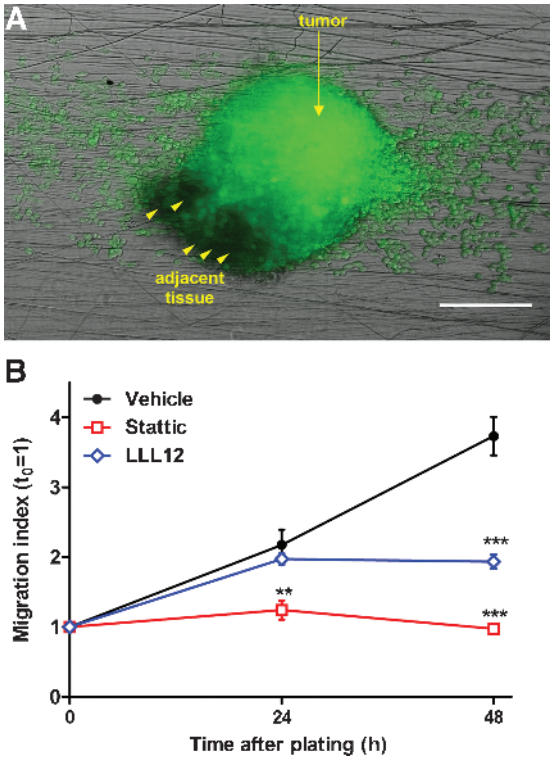

Figure 6. STAT3 inhibition reduces cell dispersion from tumor explants. (A) Representative image of a tissue explant from a GFP-expressing G9 glioma cultured on aligned nanofibers during 48 hours. Arrowheads indicate nonfluorescent areas of adjacent brain tissue. Bar, 200 μm. (B) Tumor explants were cultured in the presence of 1 μM stattic (stattic), 1 μM LLL12 (LLL12), or their vehicle (vehicle), and cell dispersion was measured as before. Both STAT3 inhibitors significantly reduced (LLL12) or abolished (stattic) outward cell migration. $^{**}P < .01$, $^{***}P < .001$ by two-way ANOVA for repeated measures.

An important finding of our study is the observation that cell motility in nanofiber scaffolds was STAT3-dependent and could be specifically disrupted with low, subtoxic concentrations of STAT3 inhibitors. This effect was reproduced with glioma cells dispersing in cultured brain slices, suggesting that migration through both types of topographically complex environments was supported by similar molecular mechanisms. Remarkably, low concentrations of STAT3 inhibitors did not affect cell motility on two-dimensional surfaces. A possible explanation for these results is that STAT3 could regulate molecular mechanisms leading to actomyosin activity in glioma cells, which is critical for three-dimensional motility but can be compensated by alternative mechanisms in two-dimensional motility [10,23]. Accordingly, low concentrations of a STAT3 inhibitor reduced the activation of a myosin regulatory chain (MLC2) only in cells cultured on nanofibers, which could explain the significant effect of partial STAT3 inhibition on three-dimensional motility and lack of effect on two-dimensional motility. In agreement, STAT3 has been implicated as a mediator of Rho GTPase signaling [50], which is critical for actomyosin contraction and tail-end retraction necessary for glioma cell movement in three-dimensional matrices [51]. Interestingly, the expression of proinvasive metalloproteases that are STAT3 targets, such as MMP2 and MMP9 [30], did not change after STAT3 inhibition on nanofibers (not shown), suggesting that the role of STAT3 was specific to regulating motility rather than invasive mechanisms in a three-dimensional context. Overall, our results show that partial inhibition of STAT3 phosphorylation is sufficient to reduce glioma cell migration, underscoring the potential of this transcription factor as a novel target for combined anti-invasive and cytotoxic strategies in gliomas.

Although we have used the nanofiber scaffolds as a novel culture model for glioma cells, it should be possible to extend these studies to other tumor cell types that disperse *in vivo* along anatomic structures, such as pancreatic, prostate, or head and neck tumors that use perineural migration for metastasis [52]. In all these cases, the topographically complex nature of nanofiber scaffolds could provide considerable advantages over other models to study three-dimensional cell migration. Whereas organotypic models (i.e., tissue slices) represent a more accurate mimicry of the microenvironment, challenging cells to migrate and invade in a manner consistent with their behavior *in vivo* [53], nanofiber scaffolds offer several practical advantages such as a simpler setup, scaling-up capability, and easy cell recovery for downstream analysis. In addition, our results suggest that, for glioma cells, migration in nanofibers and brain slices is comparable and highly sensitive to subtoxic doses of antimigratory compounds that may lack effect on rigid two-dimensional surfaces or may require much higher concentrations to elicit a comparable effect.

Finally, the possibility of measuring cell migration out of tissue explants suggests that this model could potentially be used as a bioassay for drug testing in specimens and tumorspheres derived from individual patients.

References

[1] Wen PY and Kesari S (2008). Malignant gliomas in adults. *N Engl J Med* **359**, 492–507.

[2] Louis DN (2006). Molecular pathology of malignant gliomas. *Ann Rev Pathol* **1**, 97–117.

[3] Decaestecker C, Debeir O, Van Ham P, and Kiss R (2007). Can anti-migratory drugs be screened *in vitro*? A review of 2D and 3D assays for the quantitative analysis of cell migration. *Med Res Rev* **27**, 149–176.

[4] Bellail AC, Hunter SB, Brat DJ, Tan C, and Van Meir EG (2004). Microregional extracellular matrix heterogeneity in brain modulates glioma cell invasion. *Int J Biochem Cell Biol* **36**, 1046–1069.

[5] Joy AM, Beaudry CE, Tran NL, Ponce FA, Holz DR, Demuth T, and Berens ME (2003). Migrating glioma cells activate the PI3-K pathway and display decreased susceptibility to apoptosis. *J Cell Sci* **116**, 4409–4417.

[6] Mariani L, Beaudry C, McDonough WS, Hoelzinger DB, Demuth T, Ross KR, Berens T, Coons SW, Watts G, Trent JM, et al. (2001). Glioma cell motility is associated with reduced transcription of proapoptotic and proliferation genes: a cDNA microarray analysis. *J Neurooncol* **53**, 161–176.

[7] Lamszus K, Kunkel P, and Westphal M (2003). Invasion as limitation to anti-angiogenic glioma therapy. *Acta Neurochir Suppl* **88**, 169–177.

[8] Zhai GG, Malhotra R, Delaney M, Latham D, Nestler U, Zhang M, Mukherjee N, Song Q, Robe P, and Chakravarti A (2006). Radiation enhances the invasive potential of primary glioblastoma cells via activation of the Rho signaling pathway. *J Neurooncol* **76**, 227–237.

[9] Viapiano MS and Lawler SE (2009). Glioma invasion: mechanisms and therapeutic challenges. In *CNS Cancer: Models, Prognostic Factors and Targets.* E Van Meir (Ed). Humana Press, Totowa, NJ. pp. 1219–1252.

[10] Beadle C, Assanah MC, Monzo P, Vallee R, Rosenfeld SS, and Canoll P (2008). The role of myosin II in glioma invasion of the brain. *Mol Biol Cell* **19**, 3357–3368.

[11] Johnson J, Nowicki OM, Lee CH, Chiocca AE, Viapiano MS, Lawler SE, and Lannutti JJ (2009). Quantitative analysis of complex glioma cell migration on electrospun polycaprolactone using time-lapse microscopy. *Tissue Eng Part C* **15**, 531–540.

[12] Farin A, Suzuki SO, Weiker M, Goldman JE, Bruce JN, and Canoll P (2006). Transplanted glioma cells migrate and proliferate on host brain vasculature: a dynamic analysis. *Glia* **53**, 799–808.

[13] Devarajan E and Huang S (2009). STAT3 as a central regulator of tumor metastases. *Curr Mol Med* **9**, 626–633.

[14] Lee J, Kotliarova S, Kotliarov Y, Li A, Su Q, Donin NM, Pastorino S, Purow BW, Christopher N, Zhang W, et al. (2006). Tumor stem cells derived from glioblastomas cultured in bFGF and EGF more closely mirror the phenotype and genotype of primary tumors than do serum-cultured cell lines. *Cancer Cell* **9**, 391–403.

[15] Godlewski J, Nowicki MO, Bronisz A, Williams S, Otsuki A, Nuovo G, Raychaudhury A, Newton HB, Chiocca EA, and Lawler S (2008). Targeting of the *Bmi-1* oncogene/stem cell renewal factor by microRNA-128 inhibits glioma proliferation and self-renewal. *Cancer Res* **68**, 9125–9130.

[16] Hu B, Thirtamara-Rajamani KK, Sim H, and Viapiano MS (2009). Fibulin-3 is uniquely upregulated in malignant gliomas and promotes tumor cell motility and invasion. *Mol Cancer Res* **7**, 1756–1770.

[17] Schust J, Sperl B, Hollis A, Mayer TU, and Berg T (2006). Stattic: a small-molecule inhibitor of STAT3 activation and dimerization. *Chem Biol* **13**, 1235–1242.

[18] Lin L, Hutzen B, Li PK, Ball S, Zuo M, DeAngelis S, Foust E, Sobo M, Friedman L, Bhasin D, et al. (2010). A novel small molecule, LLL12, inhibits STAT3 phosphorylation and activities and exhibits potent growth-suppressive activity in human cancer cells. *Neoplasia* **12**, 39–50.

[19] Hu B, Kong LL, Matthews RT, and Viapiano MS (2008). The proteoglycan brevican binds to fibronectin after proteolytic cleavage and promotes glioma cell motility. *J Biol Chem* **283**, 24848–24859.

[20] Sim H, Hu B, and Viapiano MS (2009). Reduced expression of the hyaluronan and proteoglycan link proteins in malignant gliomas. *J Biol Chem* **284**, 26547–26556.

[21] Wright GW and Simon RM (2003). A random variance model for detection of differential gene expression in small microarray experiments. *Bioinformatics* **19**, 2448–2455.

[22] Fraley SI, Feng Y, Krishnamurthy R, Kim DH, Celedon A, Longmore GD, and Wirtz D (2010). A distinctive role for focal adhesion proteins in three-dimensional cell motility. *Nat Cell Biol* **12**, 598–604.

[23] Ghibaudo M, Trichet L, Le Digabel J, Richert A, Hersen P, and Ladoux B (2009). Substrate topography induces a crossover from 2D to 3D behavior in fibroblast migration. *Biophys J* **97**, 357–368.

[24] Oh YM, Kim JK, Choi Y, Choi S, and Yoo JY (2009). Prediction and experimental validation of novel STAT3 target genes in human cancer cells. *PLoS One* **4**, e6911.

[25] Jiang K, Krous LC, Knowlton N, Chen Y, Frank MB, Cadwell C, Centola M, and Jarvis JN (2009). Ablation of Stat3 by siRNA alters gene expression profiles in JEG-3 cells: a systems biology approach. *Placenta* **30**, 806–815.

[26] Merchant JL (2008). What lurks beneath: IL-11, via Stat3, promotes inflammation-associated gastric tumorigenesis. *J Clin Invest* **118**, 1628–1631.

[27] Carro MS, Lim WK, Alvarez MJ, Bollo RJ, Zhao X, Snyder EY, Sulman EP, Anne SL, Doetsch F, Colman H, et al. (2010). The transcriptional network for mesenchymal transformation of brain tumours. *Nature* **463**, 318–325.

[28] Rao RD, Mladek AC, Lamont JD, Goble JM, Erlichman C, James CD, and Sarkaria JN (2005). Disruption of parallel and converging signaling pathways contributes to the synergistic antitumor effects of simultaneous mTOR and EGFR inhibition in GBM cells. *Neoplasia* **7**, 921–929.

[29] Yang F, Brown C, Buettner R, Hedvat M, Starr R, Scuto A, Schroeder A, Jensen M, and Jove R (2010). Sorafenib induces growth arrest and apoptosis of human glioblastoma cells through the dephosphorylation of signal transducers and activators of transcription 3. *Mol Cancer Ther* **9**, 953–962.

[30] Senft C, Priester M, Polacin M, Schroder K, Seifert V, Kogel D, and Weissenberger J (2011). Inhibition of the JAK-2/STAT3 signaling pathway impedes the migratory and invasive potential of human glioblastoma cells. *J Neurooncol* **101**, 393–403.

[31] Narayana A, Kunnakkat SD, Medabalmi P, Golfinos J, Parker E, Knopp E, Zagzag D, Eagan P, Gruber D, and Gruber ML (2010). Change in pattern of relapse after antiangiogenic therapy in high-grade glioma. *Int J Radiat Oncol Biol Phys* DOI: 10.1016/j.ijrobp.2010.10.038.

[32] Giese A, Bjerkvig R, Berens ME, and Westphal M (2003). Cost of migration: invasion of malignant gliomas and implications for treatment. *J Clin Oncol* **21**, 1624–1636.

[33] McKee CT, Last J, Russell P, and Murphy CJ (2011). Indentation *versus* tensile measurements of Young's modulus for soft biological tissues. *Tissue Eng Part B Rev* **17**, 155–164.

[34] Balaban NQ, Schwarz US, Riveline D, Goichberg P, Tzur G, Sabanay I, Mahalu D, Safran S, Bershadsky A, Addadi L, et al. (2001). Force and focal adhesion assembly: a close relationship studied using elastic micropatterned substrates. *Nat Cell Biol* **3**, 466–472.

[35] Yeung T, Georges PC, Flanagan LA, Marg B, Ortiz M, Funaki M, Zahir N, Ming W, Weaver V, and Janmey PA (2005). Effects of substrate stiffness on cell morphology, cytoskeletal structure, and adhesion. *Cell Motil Cytoskeleton* **60**, 24–34.

[36] Suzuki SO and Iwaki T (2005). Dynamic analysis of glioma cells: looking into "movement phenotypes". *Neuropathology* **25**, 254–262.

[37] Blando JM, Carbajal S, Abel E, Beltran L, Conti C, Fischer S, and DiGiovanni J (2011). Cooperation between Stat3 and Akt signaling leads to prostate tumor development in transgenic mice. *Neoplasia* **13**, 254–265.

[38] Sherry MM, Reeves A, Wu JK, and Cochran BH (2009). STAT3 is required for proliferation and maintenance of multipotency in glioblastoma stem cells. *Stem Cells* **27**, 2383–2392.

[39] Atkinson GP, Nozell SE, and Benveniste ET (2010). NF-κB and STAT3 signaling in glioma: targets for future therapies. *Expert Rev Neurother* **10**, 575–586.

[40] Konnikova L, Kotecki M, Kruger MM, and Cochran BH (2003). Knockdown of STAT3 expression by RNAi induces apoptosis in astrocytoma cells. *BMC Cancer* **3**, 23.

[41] Dasgupta A, Raychaudhuri B, Haqqi T, Prayson R, Van Meir EG, Vogelbaum M, and Haque SJ (2009). Stat3 activation is required for the growth of U87 cell-derived tumours in mice. *Eur J Cancer* **45**, 677–684.

[42] Li GH, Wei H, Lv SQ, Ji H, and Wang DL (2010). Knockdown of STAT3 expression by RNAi suppresses growth and induces apoptosis and differentiation in glioblastoma stem cells. *Int J Oncol* **37**, 103–110.

[43] Iwamaru A, Szymanski S, Iwado E, Aoki H, Yokoyama T, Fokt I, Hess K, Conrad C, Madden T, Sawaya R, et al. (2007). A novel inhibitor of the STAT3 pathway induces apoptosis in malignant glioma cells both *in vitro* and *in vivo*. *Oncogene* **26**, 2435–2444.

[44] Fuh B, Sobo M, Cen L, Josiah D, Hutzen B, Cisek K, Bhasin D, Regan N, Lin L, Chan C, et al. (2009). LLL-3 inhibits STAT3 activity, suppresses glioblastoma cell growth and prolongs survival in a mouse glioblastoma model. *Br J Cancer* **100**, 106–112.

[45] de la Iglesia N, Konopka G, Lim KL, Nutt CL, Bromberg JF, Frank DA, Mischel PS, Louis DN, and Bonni A (2008). Deregulation of a STAT3–interleukin 8 signaling pathway promotes human glioblastoma cell proliferation and invasiveness. *J Neurosci* **28**, 5870–5878.

[46] Gharavi NM, Alva JA, Mouillesseaux KP, Lai C, Yeh M, Yeung W, Johnson J, Szeto WL, Hong L, Fishbein M, et al. (2007). Role of the Jak/STAT pathway in the regulation of interleukin-8 transcription by oxidized phospholipids *in vitro* and in atherosclerosis *in vivo*. *J Biol Chem* **282**, 31460–31468.

[47] Tong KM, Shieh DC, Chen CP, Tzeng CY, Wang SP, Huang KC, Chiu YC, Fong YC, and Tang CH (2008). Leptin induces IL-8 expression via leptin receptor, IRS-1, PI3K, Akt cascade and promotion of NF-κB/p300 binding in human synovial fibroblasts. *Cell Signal* **20**, 1478–1488.

[48] Brantley EC and Benveniste EN (2008). Signal transducer and activator of transcription-3: a molecular hub for signaling pathways in gliomas. *Mol Cancer Res* **6**, 675–684.

[49] Senft C, Polacin M, Priester M, Seifert V, Kogel D, and Weissenberger J (2010). The nontoxic natural compound curcumin exerts anti-proliferative, anti-migratory, and anti-invasive properties against malignant gliomas. *BMC Cancer* **10**, 491.

[50] Debidda M, Wang L, Zang H, Poli V, and Zheng Y (2005). A role of STAT3 in Rho GTPase-regulated cell migration and proliferation. *J Biol Chem* **280**, 17275–17285.

[51] Salhia B, Hwang JH, Smith CA, Nakada M, Rutka F, Symons M, and Rutka JT (2008). Role of myosin II activity and the regulation of myosin light chain phosphorylation in astrocytomas. *Cell Motil Cytoskeleton* **65**, 12–24.

[52] Marchesi F, Piemonti L, Mantovani A, and Allavena P (2010). Molecular mechanisms of perineural invasion, a forgotten pathway of dissemination and metastasis. *Cytokine Growth Factor Rev* **21**, 77–82.

[53] Palfi S, Swanson KR, De BS, Chretien F, Oliveira R, Gherardi RK, Kros JM, Peschanski M, and Christov C (2004). Correlation of *in vitro* infiltration with glioma histological type in organotypic brain slices. *Br J Cancer* **91**, 745–752.

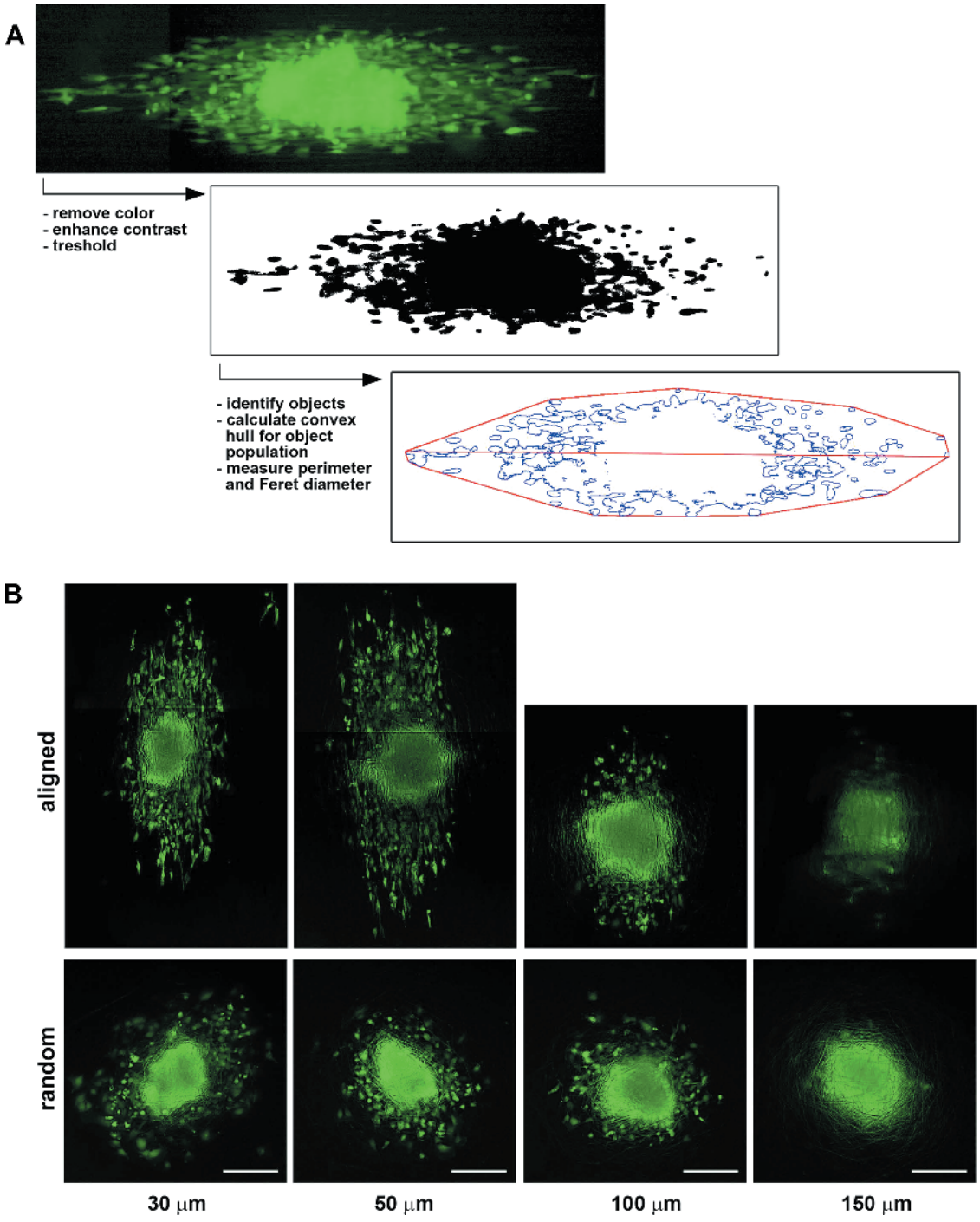

Figure W1. Analysis of cell migration on nanofiber scaffolds. (A) Images captured by fluorescence microscopy were analyzed using ImageJ software to quantify cell dispersion from the original spheroid. The maximum dispersion distance is the Feret diameter of the whole cell population at each time point. (B) Representative image of U251 glioma cells dispersing out of aggregates cultured on nanofiber scaffolds of different thickness (30-150 μm). Notice the elongated profile of cell dispersion on highly aligned nanofibers. Bars, 200 μm.

Table W1. Gene Up-regulation in Glioma Cells Migrating on Aligned Nanofibers.

Gene Symbol	Entrez Gene Name	Location	Type(s)	Fold Change	*P*
IL8	**Interleukin 8**	**Extracellular space**	**Cytokine**	**3.450**	**2.38*e* – 03**
KLF2	Kruppel-like factor 2 (lung)	Nucleus	Transcription regulator	3.080	2.98*e* – 03
CTH	Cystathionase (cystathionine gamma-lyase)	Cytoplasm	Enzyme	2.780	8.53*e* – 03
BTBD11	BTB (POZ) domain containing 11	Nucleus	Transcription regulator	2.610	4.59*e* – 04
TSLP	**Thymic stromal lymphopoietin**	**Extracellular space**	**Cytokine**	**2.490**	**9.96*e* – 03**
CBS	Cystathionine-β-synthase	Cytoplasm	Enzyme	2.450	6.64*e* – 03
TMEM158	Transmembrane protein 158 (gene/pseudogene)	Plasma membrane	Other	2.410	1.49*e* – 03
SPHK1	**Sphingosine kinase 1**	**Cytoplasm**	**Kinase**	**2.370**	**4.99*e* – 03**
MGLL	Monoglyceride lipase	Plasma membrane	Enzyme	2.340	4.76*e* – 03
NT5E	5′-Nucleotidase, ecto (CD73)	Plasma membrane	Phosphatase	2.330	1.03*e* – 03
ASNS	Asparagine synthetase (glutamine-hydrolyzing)	Cytoplasm	Enzyme	2.300	5.85*e* – 03
CXCL3	Chemokine (C-X-C motif) ligand 3	Extracellular space	Cytokine	2.250	4.44*e* – 04
PPP1R15A	Protein phosphatase 1, regulatory (inhibitor) subunit 15A	Cytoplasm	Other	2.210	7.16*e* – 03
CD55	CD55 molecule, decay accelerating factor for complement	Plasma membrane	Other	2.140	7.77*e* – 03
TRIB3	Tribbles homolog 3 (*Drosophila*)	Nucleus	Kinase	2.030	7.96*e* – 03
ALDH1A3	Aldehyde dehydrogenase 1 family, member A3	Cytoplasm	Enzyme	2.020	2.27*e* – 03
NAV3	Neuron navigator 3	Unknown	Other	1.990	8.22*e* – 04
CAMK2N1	Calcium/calmodulin–dependent protein kinase II inhibitor 1	Plasma membrane	Kinase	1.970	1.77*e* – 03
PSAT1	Phosphoserine aminotransferase 1	Cytoplasm	Enzyme	1.940	4.10*e* – 03
DUSP5	**Dual-specificity phosphatase 5**	**Nucleus**	**Phosphatase**	**1.930**	**2.05*e* – 03**
HBEGF	**Heparin-binding EGF-like growth factor**	**Extracellular space**	**growth factor**	**1.920**	**2.89*e* – 03**
RGMB	RGM domain family, member B	Plasma membrane	Other	1.900	2.42*e* – 04
CXCL2	**Chemokine (C-X-C motif) ligand 2**	**Extracellular space**	**Cytokine**	**1.890**	**1.29*e* – 03**
ADAMTS6	ADAM metallopeptidase with thrombospondine type 1 motif, 6	Extracellular space	Peptidase	1.840	5.77*e* – 03
HMGA2	High-mobility group AT-hook 2	Nucleus	Other	1.840	1.64*e* – 03
EDG1	Sphingosine-1-phosphate receptor 1	Plasma membrane	G protein–coupled receptor	1.820	3.25*e* – 04
MICAL2	Microtubule-associated monoxygenase, calponin and LIM domain containing 2	Cytoplasm	Other	1.800	1.18*e* – 03
CCND1	**Cyclin D1**	**Nucleus**	**Other**	**1.780**	**6.51*e* – 03**
EPHB2	EPH receptor B2	Plasma membrane	Kinase	1.780	1.01*e* – 03
SERPINE1	**Serpine peptidase inhibitor, clade E, member 1**	**Extracellular space**	**Other**	**1.770**	**8.82*e* – 03**
DDR2	Discoidin domain receptor tyrosine kinase 2	Plasma membrane	Kinase	1.720	3.38*e* – 03
PTHLH	Parathyroid hormone-like hormone	Extracellular space	Other	1.710	1.39*e* – 03
EMP1	Epithelial membrane protein 1	Plasma membrane	Other	1.690	4.14*e* – 03
FAM132B	Family with sequence similarity 132, member B	Unknown	Other	1.680	2.48*e* – 03
FRMD6	FERM domain containing 6	Cytoplasm	Other	1.680	4.08*e* – 03
SRGAP1	SLIT-ROBO Rho GTPase activating protein 1	Unknown	Other	1.680	6.70*e* – 04
KCNMA1	Potassium large conductance calcium-activated channel, subfamily M, alpha member 1	Plasma membrane	ion channel	1.670	9.85*e* – 04
PTPN22	Protein tyrosine phosphatase, nonreceptor type 22 (lymphoid)	Cytoplasm	Phosphatase	1.670	1.35*e* – 03
RND3	**Rho family GTPase 3**	**Cytoplasm**	**Enzyme**	**1.660**	**1.73*e* – 03**
BCAR3	Breast cancer antiestrogen resistance 3	Cytoplasm	Other	1.650	3.80*e* – 03
FLI32255	Hypothetical protein Loc643977	Unknown	Other	1.650	3.90*e* – 03
ANKRD55	Ankyrin repeat domain 55	Nucleus	Transcription regulator	1.620	2.20*e* – 03
GADD45A	Growth arrest and DNA damage–inducible, alpha	Nucleus	Other	1.620	2.25*e* – 03
PDGFA	Platelet-derived growth factor alpha polypeptide	Extracellular space	Growth factor	1.620	9.14*e* – 04
CD274	CD274 molecule	Plasma membrane	Other	1.610	4.15*e* – 04
PDCD1LG2	Programmed cell death 1 ligand 2	Plasma membrane	Other	1.610	3.80*e* – 03
F3	Coagulation factor III (thromboplastin, tissue factor)	Plasma membrane	Transmembrane receptor	1.600	1.74*e* – 03
MTHFD2	Methylenetetrahydrofolate dehydrogenase (NADP+ dependent) 2	Cytoplasm	Enzyme	1.600	7.73*e* – 03
DNER	Delta/notch–like EGF repeat containing	Plasma membrane	Transmembrane receptor	1.590	1.49*e* – 03
CEBPG	CCAAT/enhancer binding protein (C/EBP), gamma	Nucleus	Transcription regulator	1.580	6.97*e* – 03
FAM40B	Family with sequence similarity 40, member B	Unknown	Other	1.580	9.61*e* – 03
PIK3CD	**Phosphoinositide-3-kinase, catalytic, delta polypeptide**	**Cytoplasm**	**Kinase**	**1.570**	**2.64*e* – 03**
ARHGEF2	Rho/Rac guanine nucleotide exchange factor (GEF) 2	Cytoplasm	Other	1.560	5.52*e* – 03
STX1A	Syntaxin 1A (brain)	Cytoplasm	Transporter	1.560	3.76*e* – 03
TRIB1	Tribbles homolog 1 (*Drosophila*)	Cytoplasm	Kinase	1.560	2.19*e* – 03
ENOX1	Ecto-NOX disulfide-thiol exchanger 1	Unknown	Other	1.550	1.25*e* – 03
TMCC3	Transmembrane and coiled-coil domain family 3	Unknown	Other	1.550	1.42*e* – 03
GARS	Glycyl-tRNA synthetase	Cytoplasm	Enzyme	1.540	5.75*e* – 03
PIK3AP1	Phosphoinositide-3-kinase adaptor protein 1	Cytoplasm	Other	1.540	3.76*e* – 03
USP53	Ubiquitin-specific peptidase 53	Unknown	Enzyme	1.540	5.53*e* – 04
SLC38A1	Solute carrier family 38, member 1	Plasma membrane	Transporter	1.530	3.05*e* – 03
DUSP4	Dual-specificity phosphatase 4	Nucleus	Phosphatase	1.520	1.73*e* – 03
FOXQ1	Forkhead box Q1	Nucleus	Transcription regulator	1.520	1.51*e* – 03
IL11	**Interleukin 11**	**Extracellular space**	**Cytokine**	**1.520**	**8.34*e* – 04**

Table W1. (*continued*)

Gene Symbol	Entrez Gene Name	Location	Type(s)	Fold Change	*P*
MYADM	Myeloid-associated differentiation marker	Nucleus	Other	1.520	4.26*e* – 03
MB2	Metastasis-related protein mb2	Unknown	Other	1.520	5.95*e* – 03
AKAP12	**A kinase (PRKA) anchor protein 12**	**Cytoplasm**	**Transporter**	**1.510**	**6.02*e* – 03**
PHACTR2	Phosphatase and actin regulator 2	Unknown	Other	1.510	5.86*e* – 03
RASA3	RAS p21 protein activator 3	Plasma membrane	Other	1.510	1.01*e* – 04
SARS	Seryl-tRNA synthetase	Cytoplasm	Enzyme	1.510	8.21*e* – 03
FOSL1	**FOS-like antigen 1**	**Nucleus**	**Transcription regulator**	**1.510**	**1.60*e* – 03**
KLF6	Kruppel-like factor 6	Nucleus	Transcription regulator	1.510	6.73*e* – 04
RGS7	Regulator of G protein signaling 7	Cytoplasm	Enzyme	1.500	8.44*e* – 04
GEM	GTP binding protein overexpressed in skeletal muscle	Plasma membrane	Enzyme	1.500	7.04*e* – 04
IRAK2	Interleukin-1 receptor–associated kinase 2	Plasma membrane	Kinase	1.500	1.93*e* – 03
SH2D5	SH2 domain containing 5	Unknown	Other	1.500	1.76*e* – 03
WIPF3	WAS/WASL interacting protein family, member 3	Plasma membrane	Other	1.500	4.22*e* – 03

Summary of microarray data analysis (Gene Expression Omnibus data set GSE28167) showing messenger RNA up-regulation (>1.5 fold) in U251 glioma cells migrating on aligned *versus* randomly oriented nanofibers. Genes in bold face emphases have been described in the literature as regulators or targets of JAK/STAT signaling [24–26]. Results were analyzed by BRB-Array Tools software using a modified *t* test with random variance ($P < .05$ indicates statistically significant differences).

Table W2. Gene Ontology Analysis Identifies a Cell Motility Signature Upregulated in Glioma Cells Migrating on Aligned Nanofibers.

(A) Ingenuity Pathway Analysis (Ingenuity Systems)

Top Functional Networks

ID	Score	Top Functions	Upregulated Genes Associated with This Network
1	52	**Cellular movement**, hematological system development and function, hematopoiesis	*ALDH1A3*, *ARHGEF2*, *ASNS*, *CD55*, *CD274*, *CEBPG*, *CTH*, ***CXCL2***, *CXCL3*, ***DUSP5***, *F3*, *GARS*, ***HMGA2***, ***IL11***, ***IL8***, *IRAK2*, *KLF2*, *MTHFD2*, *PDGFA*, *PSAT1*, ***RND3***, ***SERPINE1***, ***SPHK1***, *TRIB3*, ***TSLP***
2	40	Tissue morphology, **cellular movement**, skeletal and muscular system development and function	***AKAP12***, *CAMK2N1*, ***CCND1***, *DDR2*, *DNER*, *DUSP4*, *EMP1*, *EPHB2*, ***FOSL1***, *GEM*, ***IL11***, *KLF6*, *PDGFA*, ***PIK3CD***, *PTHLH*, *RGS7*, *TMEM158*, *TRIB1*
3	23	Cellular development, cellular growth and proliferation, cellular function and maintenance	*BTBD11*, *DNER*, *FAM40B*, *FOXQ1*, *FRMD6*, *MGLL*, *PHACTR2*, *PTPN22*, *RASA3*, *SARS*, *SH2D5*, *USP53*
4	20	Immunologic disease, inflammatory disease, renal nephritis	*BCAR3*, *CBS*, *GADD454*, ***HBEGF***, ***IL11***, *KCNMA1*, *MICAL2*, *NT5E*, *PDCD1LG2*, *PIK3AP1*, *PPP1R15A*, *PTPN22*, *STX1A*
5	9	Cell death, cellular development, cellular growth and proliferation	*ENOX1*, *NAV3*, *RGS7*, ***SERPINE1***, *SLC38A1*, *SRGAP1*, *WIPF3*

(B) DAVID Bioinformatics Resources (NIH/NIAID):

Top Annotation Clusters

Annotation Cluster 1: Enrichment Score: 2.4295

GO Category	Term	Upregulated Genes Associated with This Cluster	*P*	Fold Enrichment
GOTERM_BP_FAT	GO:0040017~**positive regulation of locomotion**	***IL8***, *PDGFA*, *F3*, ***SPHK1***, ***HBEGF***	.00081	11.6984
GOTERM_BP_FAT	GO:0042060~wound healing	*KLF6*, *PDGFA*, *F3*, ***SERPINE1***, ***HBEGF***, ***IL11***	.00133	7.2028
GOTERM_BP_FAT	GO:0032101~regulation of response to external stimulus	***IL8***, *PDGFA*, *F3*, ***SERPINE1***, *NT5E*	.00476	7.2103
GOTERM_BP_FAT	GO:0030193~regulation of blood coagulation	*PDGFA*, *F3*, ***SERPINE1***	.01036	19.1073
GOTERM_BP_FAT	GO:0050818~regulation of coagulation	*PDGFA*, *F3*, ***SERPINE1***	.01330	16.7772

Annotation Cluster 2: Enrichment Score: 2.26307

GO Category	Term	Genes	*P*	Fold Enrichment
GOTERM_BP_FAT	GO:0040017~**positive regulation of locomotion**	***IL8***, *PDGFA*, *F3*, ***SPHK1***, ***HBEGF***	.00081	11.69834
GOTERM_BP_FAT	GO:0042060~wound healing	*KLF6*, *PDGFA*, *F3*, ***SERPINE1***, ***HBEGF***, ***IL11***	.00133	7.2028
GOTERM_BP_FAT	GO:0040012~**regulation of locomotion**	***IL8***, *PDGFA*, *F3*, ***SPHK1***, ***HBEGF***, *TRIB1*	.00136	7.1652
GOTERM_BP_FAT	GO:0030334~**regulation of cell migration**	*PDGFA*, *F3*, ***SPHK1***, ***HBEGF***, *TRIB1*	.00590	6.7836
GOTERM_BP_FAT	GO:0030335~**positive regulation of cell migration**	*PDGFA*, *F3*, ***SPHK1***, ***HBEGF***	.00654	10.3051
GOTERM_BP_FAT	GO:0051272~**positive regulation of cell motion**	*PDGFA*, *F3*, ***SPHK1***, ***HBEGF***	.00852	9.3587
GOTERM_BP_FAT	GO:0051270~**regulation of cell motion**	*PDGFA*, *F3*, ***SPHK1***, ***HBEGF***, *TRIB1*	.00935	5.9401
GOTERM_CC_FAT	GO:0009986~cell surface	*KCNMA1*, *IRAK2*, *PDGFA*, *F3*, *CD274*, ***HBEGF***	.01544	4.0069
PANTHER_PATHWAY	P00005:Angiogenesis	*PDGFA*, *DNER*, *F3*, ***PIK3CD***, ***SPHK1***, *EPHB2*	.06108	2.6626

Genes upregulated in U251 glioma cells migrating on aligned *versus* randomly oriented nanofibers (Table W1) were analyzed using Ingenuity Pathway Analysis software (A) and DAVID bioinformatics resources (B). Results from both analyses revealed a cluster of genes associated with increased cell locomotion. Genes in bold face emphases have been described in the literature as targets and/or regulators of JAK/STAT signaling.

Table W3. List of Primers Used for Quantitative RT-PCR.

Gene	Forward Sequence 5′ → 3′	Reverse Sequence 5′ → 3′
CAMK2N1	TATTGAAGATGATAGGATTG	AATTTTGACAAATAGCTGCA
CAPS	AGCTGCATTTGCCAAGCTGG	GCTGTAGTAGTCCTGGAATT
CCND1	GCGGRAGTAGGACAGGAAGTT	GAACAAACAGATCATCCGCAAAC
CXCL2	ACTGAACTGCGCTGCCAGTG	TTCTGCCCATTCTTGAGTGT
CXCL3	TCAAGAACATCCAAAGTGTG	TTGTTCAGTATCTTTTCGAT
EDG1	TATGCCAGTATGCTCTGGCT	CGATGAGTGATCCAGGCTTT
EDNRB	ATGTGTAAGCTGGTGCCTTT	TTTGGAACCCCAATTCCTTT
EMP1	ATGGAGAAGGGAAACCGGTT	GATACTGCGTTCCATCACGA
IL-8	AGACATACTCCAAACCTTTC	TCTGCACCCAGTTTTCCTTG
IL-11	AAATTCCCAGCTGACGGGGA	AAATAAATAAGATCTGGCTTTG
KLF2	GACTTAGGGTGGTAAAGGC	CATGGACAGGATGAACTCCA
MMP2	CCATCGAGACCATGCGGAAG	CCTGTATGTGATCTGGTTCTTG
MMP9	TCATCCAGTTTGGTGTCGCG	GACCACAACTCGTCGTCGTC
MMP13	GAGGTGACTGGCAAACTTGA	ATATCAGGGGTGTAATTCAC
PARP9	AAATGTCCTGTGCCTCCAAC	ACTCTGCATACCACATTGCA
PDGFA	AGTGAGGATTCTTTGGACCAC	TTGACACTGCTCGTGTTGCA
PDGFRA	TACCAGGGAGGTCAAAGAAA	TTCCTGAATCTTTTCCACAT
PI15	GATTATGCTTTTCCATATCCC	ATCCTATCCGATTGGAAGTG
RND3	AATAGAGTTGAGCCTGTGGG	ATCAGACTTGCAGCCGACCA
SERPINE1	TTTCAGAGGTGGAGAGAGCC	AAGGGAGTCTTCCACTGGCC
SESN3	GTTCATGTCAATCTACTTTT	TCATGATTTATGATCAGTAT
SOX4	TAGTTCTTGCACGCTCTTTA	TTCCCTGAAGCAGTTGATTC
SOX13	AAGGAGCTCCAGCTTCTGGT	AGGAGGTTGATCTTATGCTG
SOX21	AAGATGCACAACTCGGAGAT	CGACGAGATCTCTGCCATTT
SPHK1	CTGGTGGTCATGTCTGGAGA	CAGCAATAGCGTGCAGTTGG
STC1	TTGCATGCCTGGAAAACTCC	CCGTTGGCGATGCATTTTAA
STX1A	TCAAGTACCAGAGCAAGGC	GCAGATGATGATCATGATTT
VANGL2	AGCGTCGCTGGATTTTCTCT	ATCTCGACTCTTAGAGCGGT

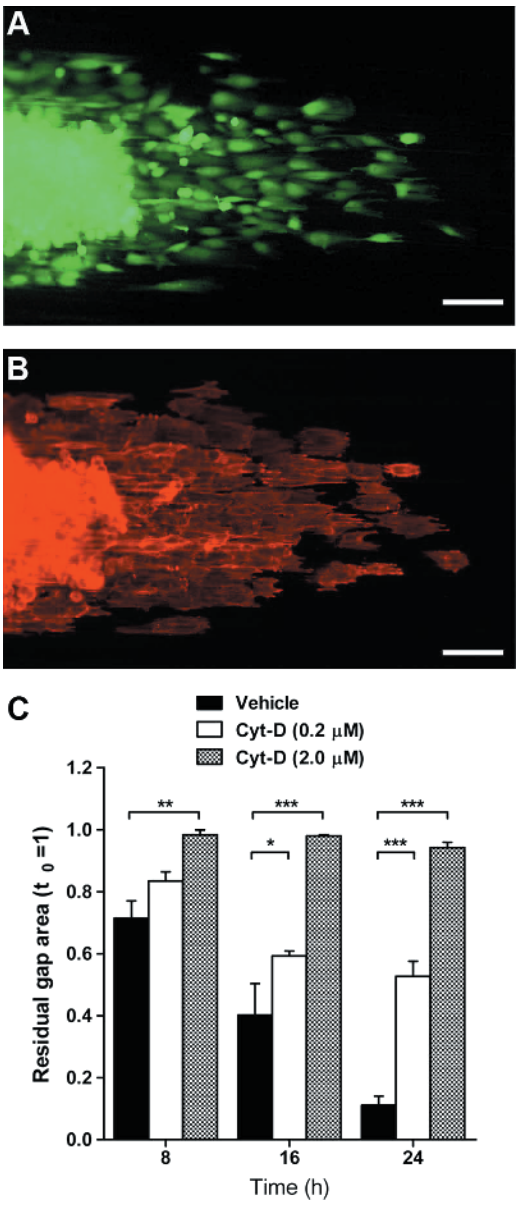

Figure W2. Inhibition of actin polymerization disrupts two-dimensional glioma cell migration. (A) Representative image of unfixed, CMFDA-labeled U251 glioma cells migrating out of a spheroid deposited on aligned nanofibers. (B) Same cells from A, imaged after fixation and staining with phalloidin–Alexa 594 to detect actin F. The staining was mostly cortical and diffuse. Bars, 100 μm. (C) Effect of cytochalasin D (Cyt-D) on the migration of U251 cells, measured using a wound healing assay. Cell migration was significantly inhibited at 2.0 μM Cyt-D and completely abolished at 2 μM due in part to cell detachment. $^{*}P < .05$, $^{**}P < .01$, $^{***}P < .001$ by two-way ANOVA for repeated measures.

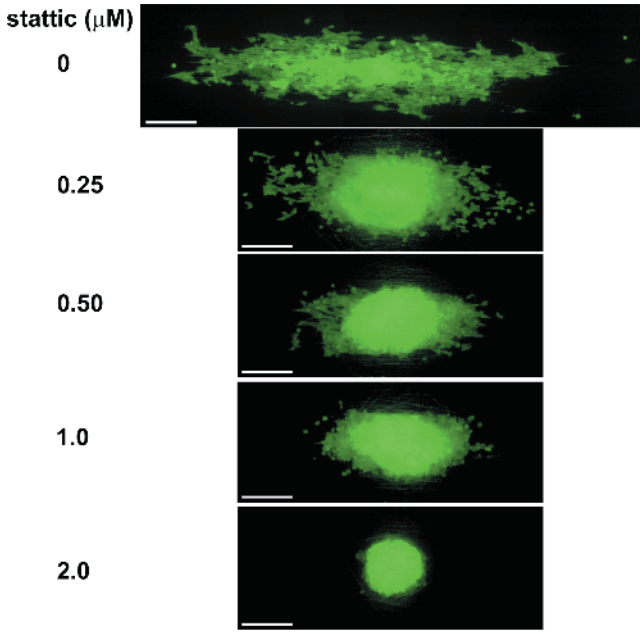

Figure W3. STAT3 inhibitors disrupt glioma cell migration. Representative images of G9 spheroids (glioblastoma-derived initiating cells) cultured on aligned nanofibers scaffolds in the presence of increasing concentrations of the STAT3 inhibitor stattic. Notice the reduction of cell dispersion along the major axis of the scaffold, without a noticeable decrease in fluorescence (ratio of integrated fluorescence/area remained approximately constant). Bars, 200 μm.

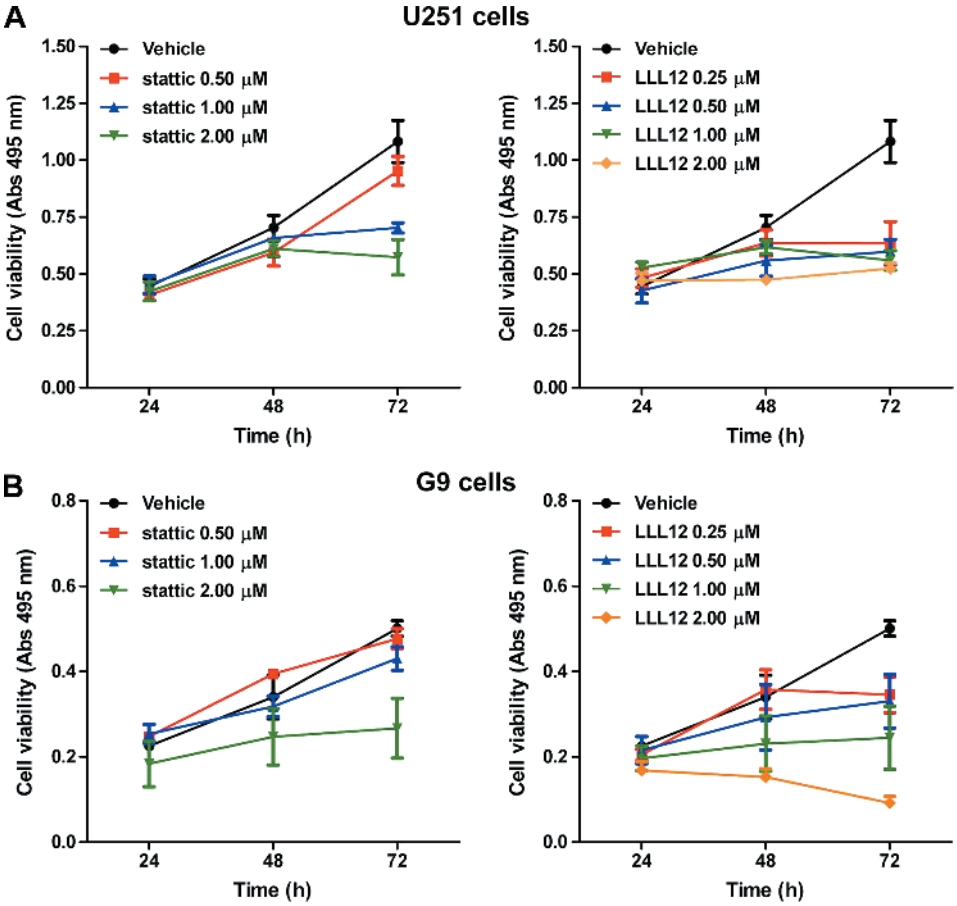

Figure W4. STAT3 inhibitors do not disrupt cell viability at early culture times. U251 (A) and G9 (B) glioma cell were cultured on aligned nanofiber for 24 to 72 hours in the presence of the STAT3 inhibitors stattic and LLL12. Toxicity of these compounds was measured using an assay for metabolic reduction of tetrazolium. Results showed that neither stattic nor LLL12 reduced cell viability in the conditions at which they inhibited cell migration (0.5-2 μM for up to 24 hours). Negative effects on cell viability were observed only at the highest concentrations tested and longer incubation times (>48 hours).

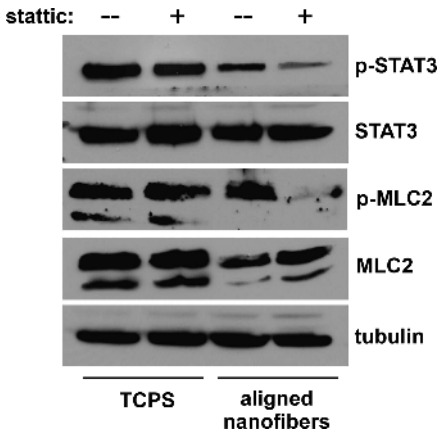

Figure W5. STAT3 inhibition reduces MLC2 phosphorylation of cells cultured on aligned nanofibers. U251 glioma cells were cultured on aligned nanofibers or TCPS for 24 hours in the presence of 1 μM stattic, collected, and processed for Western blot analysis. Results showed that a low concentration of the STAT3 inhibitor partially reduced STAT3 phosphorylation in cells of myosin II, MLC2. In contrast, neither STAT3 nor MLC2 phosphorylation was affected by the same treatment when cells were cultured on TCPS.

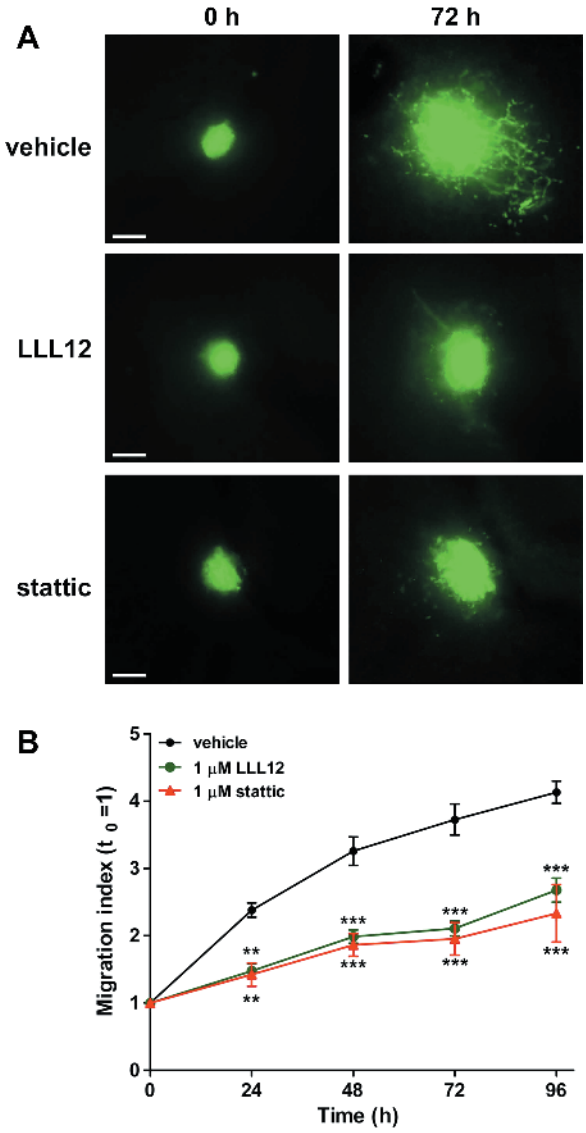

Figure W6. STAT3 inhibition reduces cell dispersion in cultured brain slices. G9 glioma cells were treated with 1 μM stattic of 1 μM LLL12 overnight and deposited on brain slices prepared as described in the Materials and Methods section. Dispersion of the cells in the tissue slice was followed by fluorescence microscopy for 96 hours. (A) Cell migration followed a pattern of dispersion with typical trails of cells dispersing out of tumorspheres, which was abolished by the pharmacological treatments. (B) Quantitative results indicated that cell dispersion had been significantly reduced by treatment with low concentrations of the STAT3 inhibitors, in agreement with the results observed using nanofiber scaffolds. $^{**}P < .01$, $^{***}P < .001$ by two-way ANOVA for repeated measures. Bars, 200 μm.